

# Self-Supported Nano-WO<sub>3</sub> Foams formed by Self-Assembly of Non-Woven Mats

Gagan Jodhani<sup>1</sup>, Selda Topcu<sup>1</sup>, Aisha Bishop-Haynes<sup>1,2</sup>, Jusang Lee<sup>1</sup> and Pelagia Irene Gouma<sup>1,3,4\*</sup>

<sup>1</sup>Department of Materials Science and Engineering, Stony Brook University, Stony Brook, NY, 11794

<sup>2</sup>Analysis and Evaluation Technology Division, U.S. Army ARDEC RDAR-MEF-E, Building 94, 2nd Floor, Picatinny, N.J. 07806-5000

<sup>3</sup>Department of Materials Science & Engineering, University of Texas at Arlington, Arlington, TX, 76019

<sup>4</sup>Institute of Predictive Performance Methodologies, University of Arlington Research Institute, Fort Worth, TX, 76118  
Email: pelagia.gouma@uta.edu

**Abstract:** Self-supported tungsten oxide (WO<sub>3</sub>) foams were synthesized by a combination of sol-gel, electrospinning, and thermal oxidation processes. Mixtures of tungsten isopropoxide (C<sub>18</sub>H<sub>42</sub>O<sub>6</sub>W)-based precursors and cellulose acetate (CA) were electrospun and subsequently heat-treated. Structural characterization of the as-processed foam-like monoliths confirmed that they consist of cubic WO<sub>3</sub> nanoparticles in a continuous matrix with open porosity. The formation of the self-supported nano-foams is a result of self-assembly of the composite nanofibers in the non-woven electrospun mats. The cubic WO<sub>3</sub> foams have a band-gap of 2.53eV and can be used as visible light photocatalysts.

**Keywords:** Electrospinning, metal oxide, nano foams, self-supported, photocatalysts.

## 1. Introduction

Self-supported nanostructures have gained increasing attention recently for use in functional applications instead of dispersed nanoparticles; these include photocatalysis [1, 2], electrochemical energy storage [3], and gas sensing [4]. Among the various self-supported architectures reported, foam structures stand out. Various techniques have been reported to-date to obtain metal oxide foam architectures, including coating of metal foams with metal oxides, polymer-metal oxide composite foams, and pure metal oxide foam structures. The reported techniques for synthesizing pure foams usually require complex processing. For example templating [5, 6] involves filling the mold matrix with metal oxide sol and using calcination or combustion to obtain foams. Thermal treatment of pure metal blocks uses precursors that are typically costly [7]. In this study, a straightforward and cost-effective route to produce metal oxide foams is explored involving the electrospinning process. Tungsten trioxide was chosen as candidate for the study as it finds diverse applications (as visible light photocatalyst, gas sensor, electrochromic material, etc.) and occurs in a variety of polymorphs. Electrospinning of self-supported metal oxide nanofibrous architectures was demonstrated earlier by our group [8-10]. Blend electrospinning involving tungsten isopropoxide (C<sub>18</sub>H<sub>42</sub>O<sub>6</sub>W) and cellulose acetate, is explored in this work to produce nanostructured foams of WO<sub>3</sub>.

## 2. Experimental Methods:

WO<sub>3</sub> sol was prepared using tungsten isopropoxide (All Chemie Ltd.) as a precursor to blend electrospinning. The sol was prepared with 0.2M concentration in butanol and was subjected to ultrasonic mixing and 48h aging, to allow sufficient time for butoxide substitution. A solution of 0.1M cellulose acetate (CA) (Aldrich 419028) in 40% acetic acid and 60% acetone was prepared; the aged sol was mixed with CA solution in the ratio of 1:4 respectively. The resultant solution was prepared for electrospinning and the resulting as-spun mats were heat treated at 375°C for 8h; the heating and cooling rate were set at 175°C/h.

To study the effect of electrospinning on formation of foam structures, thin films were formed on glass substrate by spin coating. Layer formation on the substrate occurred in 2 cycles. For the first cycle the spin coating parameters were 1000RPM for 9 seconds and for the second cycle the parameters were 200 RPM for 20 seconds. The thickness of the film was controlled by the number of layers deposited on the substrate (1-3). Each layer was completely dried before the next layer was deposited on top. The spin-coated thin films were subjected to the same thermal treatment as the electrospun samples. Scanning Electron microscopy (SEM, LEO 1550) was conducted on the electrospun and spin coated samples. The electrospun samples, obtained upon thermal treatment, were further characterized using transmission electron microscopy (TEM, JEOL 1400), selected area diffraction (SAED), X-ray Diffraction (XRD, Rigaku Miniflex II) and UV-Vis Spectrometer (Jasco J-815).

### 3. Results

Figure 1 below shows the XRD patterns of the  $\text{WO}_3$  foams. The peaks obtained come from two phases and were matched to the cubic  $\text{WO}_3$  (JCPDS 41-905) and a non-stoichiometric oxide of tungsten  $\text{WO}_{2.9}$  (JCPDS 18-1417). Formation of cubic  $\text{WO}_3$  has earlier been reported by our group when annealing the as-spun mats at these temperatures[11]. The formation of non-stoichiometric phase is attributed to an oxygen deficient environment occurring during polymer degradation upon heat-treatment. The relative phase distribution is 60% cubic  $\text{WO}_3$  and 40% tetragonal  $\text{WO}_{2.9}$ , based on the relative peak intensities from the XRD pattern.

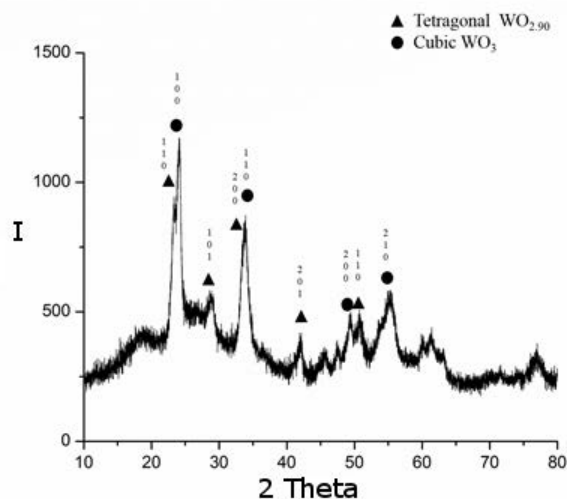
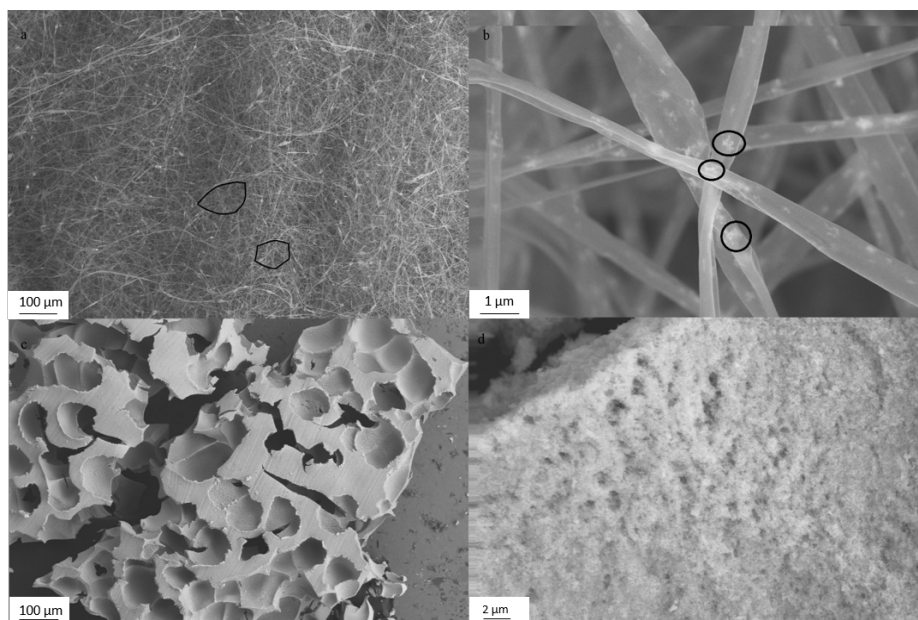


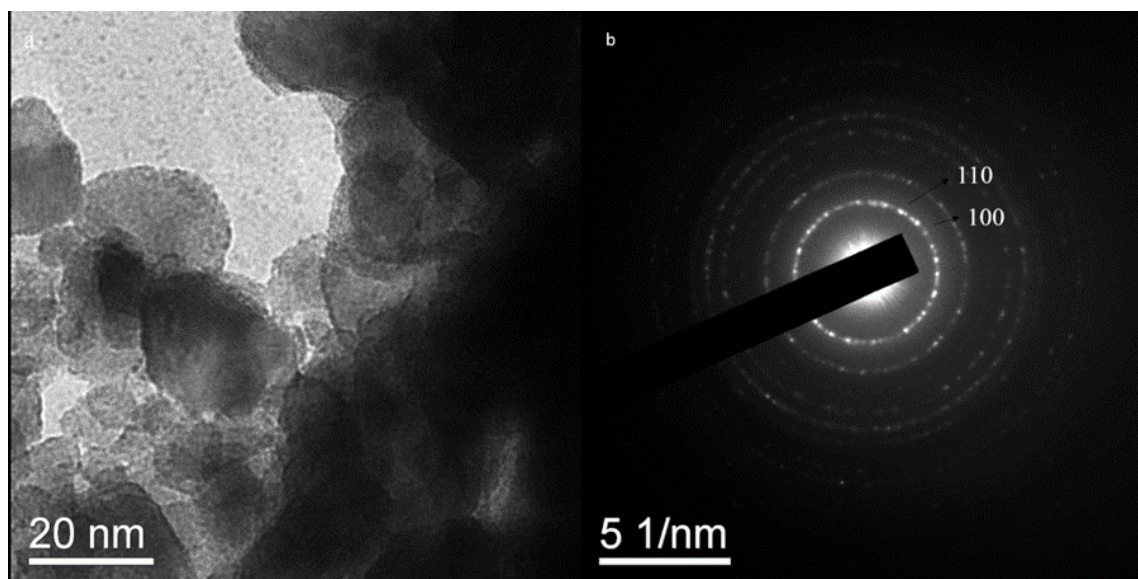
Figure 1. X-ray Diffraction pattern for foam structure

Figure 2a below shows the Scanning Electron Micrographs for as spun CA-sol-gel nanofibers. Bead formation is seen on the fibers, the formation of beads being the result of a viscous gel formed by the polymer and oxide precursor. Figure 2c shows Scanning Electron Micrographs of the heat-treated samples that further reveal the foam structure. Highly porous foams with a large pore density were obtained by the calcination of the electrospun mats. Typical pore sizes were in the range of 50-70 $\mu\text{m}$ .



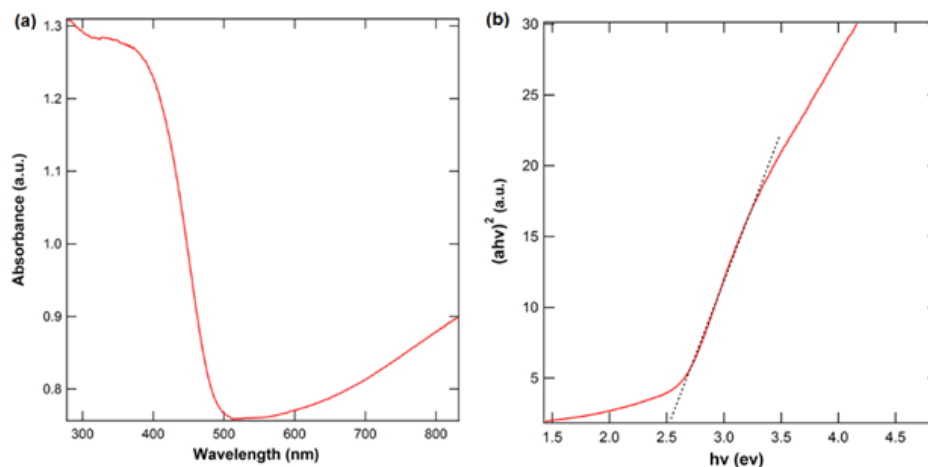
**Figure 2:** a) SEM image of as spun fibers, highlighting the formation of honeycomb structures b) High magnification SEM image of fibers highlighting the sol particles in the fibers c) SEM image of foam structures obtained after thermal treatment at 375°C d) High magnification SEM image of foam surface showing the agglomerated sol particles and nano porosity.

Figure 3a and 3b show TEM micrographs and SAED patterns for the thermally- treated material. Highly crystalline  $\text{WO}_3$  grains of 20-30nm could be observed inside the foam matrix. A dense distribution of nano sized pores was also observed inside the matrix. The electron diffraction pattern (Fig. 3b) show rings that correspond to the cubic phase of  $\text{WO}_3$  (JCPDS #41-905) and match with XRD analysis results.



**Figure 3:** (a, b) TEM images and SAED pattern of foam structure respectively

Optical absorption spectra of the  $\text{WO}_3$  foam are shown in Fig. 4a. The light absorption spectrum and the band gap energy of the samples were calculated using the formula  $(\alpha h\nu)^2 = A(h\nu - E_g)$ . This equation applies to a direct band gap materials. ( $\alpha$ : absorption coefficient,  $h$ : Planck constant =  $6.63 \times 10^{-34}$  J s,  $\nu$ : light frequency,  $E_g$ : band gap and  $A$ : constant with a value of 1, respectively [12]). The value of the band gap ( $E_g$ ) is obtained by extrapolating the slope of the  $(\alpha h\nu)^2 - h\nu$  plot to where it crosses the x axis (as shown in Fig 4b). Thus, the value of  $E_g$  is estimated to be 2.53 eV for this material. The band gap is the lowest reported for  $\text{WO}_3$  nanostructures. The foam, thus, absorbs light with wavelengths in the visible part of the solar spectrum.



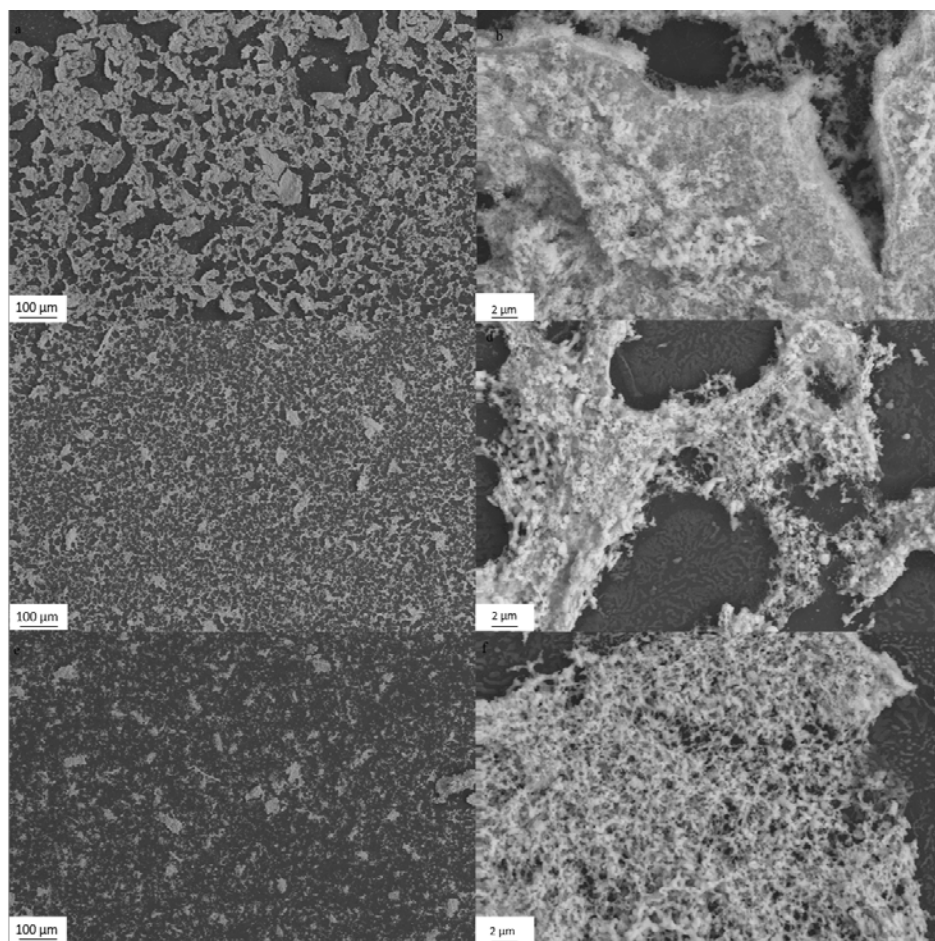
**Figure 4:** (a) UV-Vis absorption spectra of foam (b) the plot of band gap energy and  $(\alpha h\nu)^2$  of  $\text{WO}_3$  foam

**Table 1.** Reported Band Gap values for  $\text{WO}_3$  Structures

Material	Morphology	Polymorph	Band Gap, eV	Reference
Commercial $\text{WO}_3$ (Sigma Aldrich)	Nanoparticles	Monoclinic	2.61	[13]
$\text{WO}_3$	flake shaped particles	Monoclinic	2.6	[14]
$\text{WO}_3$	Nanospheres	Monoclinic	2.53	[15]
$\text{WO}_3$	Nanoplates	Orthorhombic	2.73	[15]
$\text{WO}_3$	Nanorods	Hexagonal	3.12	[15]
$\text{WO}_3$	3D Nanoporous Films	Orthorhombic	2.73	[16]

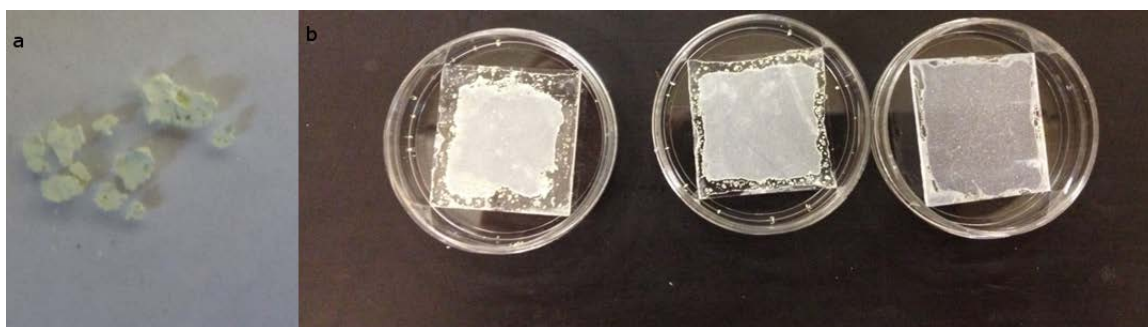
Comparison with spin-coated films

Figure 5 shows the SEM images for the spin-coated films. As the number of layers increased, the distribution of particles on the surface of the substrate increased upon heat-treatment. This corresponds to a higher amount of sol being present in the thicker films. Upon thermal treatment and degradation of polymer, the metal oxide film appears to have collapsed and the nanoparticles are now randomly distributed all over the substrate.



**Figure 5:** SEM image of thermally treated spin coated films coated (a,b) 3 times, (c,d) 2 times (e,f) 1 time

Whereas self-supported foams were obtained via the electrospinning process, loose powder networks were seen on the as-spun samples. Figure 6 compares and contrasts the morphologies of (a) foams obtained upon heat treatment of electrospun mats and (b) heat treated thin films.



**Figure 6:** (a) Self-supported foam structures obtained from electrospun mats (b) thermally treated spin coated films, coated 3, 2 and 1 times (L to R).

## 4. Discussion

The foam structure has likely resulted from the formation of a thick, viscous gel by the sol+CA solution used for electrospinning. The gel formation was the outcome of the interaction of the polymer with metal oxide sol. Such polymer-metal oxide interaction has been reported earlier for hydrated zirconia (HZ)/alumina(HA) with PVP[17]. It was observed that the addition of PVP enhanced the crystallization and dehydration of HZ/HA. The interaction between the PVP and HZ/HA changed during the dehydration process where formation of poly-N-butyl- $\gamma$ -aminobutyric acid was observed instead. Upon thermal treatment of the mixture at 500°C, pure metal oxides were obtained without any carbon traces.

In this study the polymer-sol gel interactions resulted in a non-homogenous solution. Upon electrospinning beaded fibers were noticed; the formation of beads were partly due to the lack of homogeneity in the solution. Figure 2b is a high magnification image revealing a high concentration of the sol-gel material within the polymer beads. Figure 2a highlights in black polygonal areas of porosity outlined by a high density of beads. The shape and area of these polygons are consistent with the shape and size of the large pores in the foam. Previous work by Schlatter et al. [18] has described the formation of self-assembled honeycomb structures in electrospun polymers. Beads or thicker fibers typically “framed” the walls in these structures.

In the case of CA+sol electrospun mats, when subjected to thermal treatment at 375°C, the polymer component melts between 170-240°C and breaks down at 370°C to water, carbon oxides (CO and CO<sub>2</sub>) and methane under an oxidative atmosphere[19]. Upon the polymer decomposition, the sol particles agglomerate to form a dense structure while maintaining a nano structure and nano- sized surface porosity (fig 2d). The macroscopic porosity seen in the foams can be attributed to the honeycomb structures formed during the self-assembly of electrospun mats.

## 5. Conclusion

We have successfully demonstrated the synthesis of self-supported WO<sub>3</sub> foams via the self-assembly of electrospun fibers. The foams have a band gap of 2.53eV and can be used as visible light photocatalysts.

**Acknowledgements.** This work has been sponsored by US Army contract award# W15QKN-13-P-0014. Research carried out in part at the Center for Functional Nanomaterials, Brookhaven National Laboratory, which is supported by the U.S. Department of Energy, Office of Basic Energy Sciences, under Contract No. DE-SC0012704. We thank Jing Zhang for her contribution towards this project.

## References

1. P. I. Gouma and J. Lee, "Photocatalytic nanomats clean up produced water from fracking," *Translational Materials Research*, vol. 1, p. 025002, 2014.
2. S. Topcu, G. Jodhani, and P. Gouma, "Optimized nanostructured TiO<sub>2</sub> photocatalysts," *Frontiers in Materials*, vol. 3, 2016-July-22 2016.
3. C. Yuan, J. Li, L. Hou, X. Zhang, L. Shen, and X. W. Lou, "Ultrathin Mesoporous NiCo<sub>2</sub>O<sub>4</sub> Nanosheets Supported on Ni Foam as Advanced Electrodes for Supercapacitors," *Advanced Functional Materials*, vol. 22, pp. 4592-4597, 2012.
4. A. Walcarius, "Template-directed porous electrodes in electroanalysis," *Analytical and Bioanalytical Chemistry*, vol. 396, pp. 261-272, Jan 2010.
5. D. Walsh, L. Arcelli, T. Ikoma, J. Tanaka, and S. Mann, "Dextran templating for the synthesis of metallic and metal oxide sponges," *Nat Mater*, vol. 2, pp. 386-390, 06//print 2003.

6. H. Maekawa, J. Esquena, S. Bishop, C. Solans, and B. F. Chmelka, "Meso/Macroporous Inorganic Oxide Monoliths from Polymer Foams," *Advanced Materials*, vol. 15, pp. 591-596, 2003.
7. E. S. Park and S. D. Postle, "Ceramic foams," ed: Google Patents, 1989.
8. K. M. Sawicka and P. Gouma, "Electrospun composite nanofibers for functional applications," *Journal of Nanoparticle Research*, vol. 8, pp. 769-781, 2006/12/01 2006.
9. K. M. Sawicka, A. K. Prasad, and P. I. Gouma, "Metal Oxide Nanowires for Use in Chemical Sensing Applications," *Sensor Letters*, vol. 3, pp. 31-35, // 2005.
10. G. Wang, Y. Ji, X. Huang, X. Yang, P.-I. Gouma, and M. Dudley, "Fabrication and Characterization of Polycrystalline WO<sub>3</sub> Nanofibers and Their Application for Ammonia Sensing," *The Journal of Physical Chemistry B*, vol. 110, pp. 23777-23782, 2006/11/01 2006.
11. S. Sood, K. Kisslinger, and G. P, "Nanowire Growth by an Electron-Beam-Induced Massive Phase Transformation," *JOURNAL OF THE AMERICAN CERAMIC SOCIETY*, vol. 97, pp. 3733-3736, 2014.
12. Z. Xu, I. Tabata, K. Hirogaki, K. Hisada, T. Wang, S. Wang, et al., "Preparation of platinum-loaded cubic tungsten oxide: A highly efficient visible light-driven photocatalyst," *Materials Letters*, vol. 65, pp. 1252-1256, 2011.
13. Y. Wicaksana, S. Liu, J. Scott, and R. Amal, "Tungsten Trioxide as a Visible Light Photocatalyst for Volatile Organic Carbon Removal," *Molecules* pp. 19, 17747-17762, 2014.
14. E. Luevano-Hipolito, A. M.-d. I. Cruz, E. Lopez-Ceallar, O.L.Yu, and H. Brouwers, "Synthesis, characterization and photocatalytic activity of WO<sub>3</sub>/TiO<sub>2</sub> for NO removal under UV and visible light irradiation," *Materials Chemistry&Physics*, pp. 208-213, 2014.
15. M. Farhadiana, P. Sangpouta, and G. Hosseinzadeh, "Morphology dependent photocatalytic activity of WO<sub>3</sub> nanostructures," *Journal of Energy Chemistry*, pp. 171-177, 2015.
16. J. Z. Oua, R. A. Rania, S. Balendhrana, A. S. Zoolfakara, M. R. Fieldb, S. Zhuiykovc, et al., "Anodic formation of a thick three-dimensional nanoporous WO<sub>3</sub> film and its photocatalytic property," *Electrochemistry Communications*, pp. 128-132, 2013.
17. T. M. Zima, I. A. Vorsina, and N. Z. Lyakhov, "Interaction of poly-N-vinylpyrrolidone with hydrated metal oxides," *Inorganic Materials*, vol. 45, pp. 524-532, 2009/05/01 2009.
18. D. Ahirwal, A. Hebraud, R. Kadar, M. Wilhelm, and G. Schlatter, "From self-assembly of electrospun nanofibers to 3D cm thick hierarchical foams," *Soft Matter*, vol. 9, pp. 3164-3172, 2013.
19. M. d. C. C. Lucena, A. E. V. de Alencar, S. E. Mazzeto, and S. d. A. Soares, "The effect of additives on the thermal degradation of cellulose acetate," *Polymer Degradation and Stability*, vol. 80, pp. 149-155, // 2003.